Few-cycle-laser-pulse-assisted electron-ion radiative recombination

A. Čerkić[1] and D. B. Milošević[1,2,3]

[1]*Faculty of Science, University of Sarajevo, Zmaja od Bosne 35, 71000 Sarajevo, Bosnia and Herzegovina*

[2]*Max-Born-Institut, Max-Born-Strasse 2a, 12489 Berlin, Germany*

[3]*Academy of Sciences and Arts of Bosnia and Herzegovina, Bistrik 7, 71000 Sarajevo, Bosnia and Herzegovina*

(Received 15 July 2013; published 16 August 2013)

Electron-ion radiative recombination assisted by a few-cycle laser pulse is analyzed in the frame of the *S*-matrix theory. The result obtained in the first Born approximation corresponds to the direct recombination of electrons with ionic targets, while the result in the second Born approximation corresponds to the recombination preceded by electron-ion scattering. Driven by the laser pulse, the once scattered electron may return to the same ion and recombine with it. The x-ray photon emitted in such a process may have high energies. The dependence of the energy spectrum on various parameters, such as the carrier-envelope phase, peak intensity, and duration of the laser pulse, and the incident electron energy and angle, is investigated. The abrupt cutoffs of the plateau structures in the energy spectra of the process are explained by classical analysis.

DOI: 10.1103/PhysRevA.88.023414 PACS number(s): 34.80.Qb, 32.30.Rj, 34.80.Lx, 33.20.Xx

I. INTRODUCTION

The generation of ultraviolet radiation and soft x rays in various processes involving the interaction of a strong laser field with matter has been a very important subject of research over the past few decades. Some of the atomic processes that result in the production of high-energy photons are high-order harmonic generation (HHG) [1,2], laser-induced bremsstrahlung [3], laser-assisted x-ray–atom scattering [4–6], and laser-assisted electron-ion recombination (LAR) [7,8]. Electron-ion recombination assisted by a few-cycle laser pulse is analyzed in the present paper.

The process of electron-ion recombination is very important in plasma physics and astrophysics (for a review and more references, see Sec. II C in Ref. [9]). The radiative recombination is a special case of this process, where the energy is transferred from the free electron to the photon, which acts as a third body in the process. In the laser-assisted radiative electron-ion recombination, the incident electron may absorb (emit) the energy from (to) the laser field, before it recombines with the target ion. As a result, a high-energy photon is emitted. This is the process of direct recombination and we denote it as LAR. It can also happen that the incident electron scatters on an ion in the laser field. The scattered electron, driven by the laser field, may then return to the same ion and recombine with it. This process is denoted as SLAR, where "S" stands for "scattering." The x-ray photons emitted in the SLAR process may have higher energies than those emitted in the LAR process.

The LAR process in infinitely long pulses was analyzed in Refs. [7,8,10,11]. In Ref. [11], an analytical model for electron–H^+-ion recombination was introduced, where the *S*-matrix element was constructed from an exact electron Coulomb-Volkov wave function and an approximate laser-modified hydrogen state.

The laser-assisted recombination including the scattering effects (SLAR) in infinitely long pulses was investigated in Refs. [12–15]. In particular, resonant enhancements in cross sections for laser-assisted radiative electron–H-atom attachment were obtained in Ref. [15]. These enhancements occur for incident electron energies at which the electron can be attached by emitting a photon of the energy equal to an integer number of laser photons.

In Ref. [13] the dependence of the energy spectra on the relative phase between two field components of the linearly polarized bichromatic laser field was analyzed. A similar analysis is presented in this paper, where we investigate the dependence of the energy spectra on the carrier-envelope phase (CEP) of the few-cycle laser pulse. The CEP is the relative phase between the maximum of the pulse envelope and the nearest maximum of the carrier wave. The LAR process in few-cycle pulses was considered earlier in Refs. [16–18]. In Refs. [17,18], direct recombination was analyzed using the *S*-matrix theory, with the electron continuum state described by the Coulomb-Volkov wave function. It has been found that the emitted photon spectrum is affected by both the number of optical cycles and the CEP [17]. It has been also concluded that the spectrum width depends on the CEP and the pulse peak intensity [18]. In Ref. [16] it was shown that x rays in LAR process are generated during only a very short time interval (small fraction of the laser period) so that attosecond pulses can be generated in this process.

There is a small number of experiments concerning the laser-assisted electron-ion recombination. We mention here some recent experimental findings on electron-ion recombination [19,20]. In Ref. [19], phase-dependent electron-ion recombination was observed. The polarization dependence of electron–D^+-ion recombination was investigated in Ref. [20]. On the other hand, there are much more experimental data on high-order harmonic generation, a process that is related to the laser-assisted electron-ion recombination. In the HHG process, an atom is ionized by a strong laser field. The released electron moves in the laser field and returns to the parent ion, recombining with it. The final result is the emission of a high-energy photon. This is a three-step process, just like SLAR. The HHG and SLAR processes differ only in the first step (ionization in HHG vs scattering of an electron in SLAR), while the second and third step (moving of a free electron in the field and recombination) are identical. HHG has been extensively explored, both in theory and experiment, in the past two decades. In Refs. [21,22], it has been shown that

accurate photorecombination cross sections of the atoms in the field-free condition can be extracted from the HHG spectra obtained by few-cycle laser pulses. In Refs. [23,24], these photorecombination cross sections were actually extracted from experimental HHG data.

In this paper, we analyze both the LAR and SLAR processes in a few-cycle laser pulse. These introductory remarks are followed by the quantum-mechanical theory based on the S-matrix formalism that is presented in Sec. II. Our classical analysis is described in Sec. III, while Sec. IV contains the numerical results. Finally, the conclusions are summarized in Sec. V. The atomic system of units ($\hbar = e = m_e = 4\pi\varepsilon_0 = 1$) is used throughout the paper.

II. *S*-MATRIX THEORY FOR FEW-CYCLE PULSES

The total Hamiltonian of the laser-assisted electron-ion recombination is

$$\begin{aligned} H(t) &= H_0(t) + V_{\rm X}(\mathbf{r},t), \\ H_0(t) &= -\frac{\boldsymbol{\nabla}^2}{2} + V(\mathbf{r}) + V_{\rm L}(t), \end{aligned} \tag{1}$$

where $\boldsymbol{\nabla} \equiv \partial/\partial\mathbf{r}$, $V(\mathbf{r})$ is the atomic binding potential, $V_{\rm L}(t)$ is the laser-atom interaction, and $V_{\rm X}(\mathbf{r},t)$ is the interaction of the atom with the x-ray field. We use the length gauge and the dipole approximation, so that $V_{\rm L}(t) = \mathbf{r}\cdot\mathbf{E}_{\rm L}(t)$ and $V_{\rm X}(\mathbf{r},t) = \mathbf{r}\cdot\mathbf{E}_{\rm X}(\mathbf{r},t)$, where $\mathbf{E}_{\rm L}(t)$ and $\mathbf{E}_{\rm X}(\mathbf{r},t)$ are the electric field vectors of the laser pulse and x-ray radiation, respectively. We suppose that the few-cycle laser pulse is linearly polarized along the z axis, with a sine-squared envelope. In that case, the electric field vector of the few-cycle laser pulse is given by

$$\mathbf{E}_{\rm L}(t) = E_0 \sin^2\left(\frac{\pi t}{T_{\rm p}}\right)\cos(\omega t + \phi)\hat{\mathbf{e}}_{\rm L}, \quad t \in [0, T_{\rm p}], \tag{2}$$

where $E_0 = I^{1/2}$ is the laser field amplitude (I is the laser intensity), $T_{\rm p}$ is the pulse duration, ω is the angular frequency, ϕ is the carrier-envelope phase (CEP) of the pulse, and $\hat{\mathbf{e}}_{\rm L}$ is the unit polarization vector of the laser field. We also suppose that the pulse length is equal to an integer number $n_{\rm p}$ of optical cycles $T = 2\pi/\omega$, i.e., $T_{\rm p} = n_{\rm p}T$. We consider the x-ray radiation field as quantized, so that

$$\mathbf{E}_{\rm X}(\mathbf{r},t) = \mathbf{E}_{\rm X}^{(+)}(\mathbf{r},t) + \mathbf{E}_{\rm X}^{(-)}(\mathbf{r},t), \tag{3}$$

$$\mathbf{E}_{\rm X}^{(+)}(\mathbf{r},t) = iC_{\mathbf{K}}\hat{\mathbf{e}}_{\mathbf{K}}a_{\mathbf{K}}e^{-i(\omega_{\mathbf{K}}t - \mathbf{K}\cdot\mathbf{r})}, \tag{4}$$

$$\mathbf{E}_{\rm X}^{(-)}(\mathbf{r},t) = -iC_{\mathbf{K}}\hat{\mathbf{e}}_{\mathbf{K}}a_{\mathbf{K}}^{\dagger}e^{i(\omega_{\mathbf{K}}t - \mathbf{K}\cdot\mathbf{r})}, \tag{5}$$

where $a_{\mathbf{K}}$ and $a_{\mathbf{K}}^{\dagger}$ are the photon annihilation and creation operators of the x-ray field, $\mathbf{K}$, $\omega_{\mathbf{K}}$, and $\hat{\mathbf{e}}_{\mathbf{K}}$ are the wave vector, energy, and unit polarization vector of the emitted x-ray photon, respectively, and $C_{\mathbf{K}}^2 = 2\pi\omega_{\mathbf{K}}/\mathcal{V}$ with $\mathcal{V}$ representing the quantization volume.

The general form of the S matrix is

$$S_{\rm fi} = i\lim_{\substack{t'\to\infty \\ t\to-\infty}} \langle\Phi_{\rm out}(t')|G(t',t)|\Phi_{\rm in}(t)\rangle, \tag{6}$$

where $G \equiv G^{(+)}$ is the total retarded time-dependent Green's operator that corresponds to the Hamiltonian $H(t)$ and satisfies the integral equation

$$G(t',t) = G_0(t',t) + \int_t^{t'} dt''G(t',t'')V_{\rm X}(\mathbf{r},t'')G_0(t'',t), \tag{7}$$

with Green's operator $G_0 \equiv G_0^{(+)}$ corresponding to the Hamiltonian $H_0(t)$. The state $\Phi_{\rm in}$ in Eq. (6) is the initial electron state in the absence of the laser field multiplied by the vacuum state $|0_{\mathbf{K}}\rangle$ of the x-ray field, while $\Phi_{\rm out}$ represents the bound electron state (in the absence of the laser field) multiplied by the one-photon state $|1_{\mathbf{K}}\rangle$ of the x-ray field. If we use Eq. (7) and relations (see Ref. [12] and references therein)

$$\begin{aligned} iG_0(t',t)|\Phi_{\rm in}(t)\rangle &= |\Psi_{\mathbf{p}}(t')\rangle|0_{\mathbf{K}}\rangle, \\ \langle\Phi_{\rm f}(t')| &= i\langle\Phi_{\rm out}(t)|G(t,t'), \end{aligned} \tag{8}$$

in Eq. (6), we obtain

$$S_{\rm fi} = -i\lim_{\substack{t'\to\infty \\ t\to-\infty}} \int_t^{t'} dt''\langle\Phi_{\rm f}(t'')|\mathbf{r}\cdot\mathbf{E}_{\rm X}^{(-)}(\mathbf{r},t'')|\Psi_{\mathbf{p}}(t'')\rangle|0_{\mathbf{K}}\rangle, \tag{9}$$

where $|\Psi_{\mathbf{p}}(t)\rangle$ is the solution of the Schrödinger equation for the Hamiltonian $H_0(t)$ defined by Eq. (1). We suppose that the atomic potential is $V = V_{\rm C} + V_{\rm S}$, where $V_{\rm C}$ is the Coulomb potential and $V_{\rm S}$ is a short-range potential. The splitting of the Hamiltonian $H_0 = (H_0 - V_{\rm S}) + V_{\rm S}$ leads to the Lippmann-Schwinger equation

$$|\Psi_{\mathbf{p}}(t)\rangle = |\Psi_{\mathbf{p},{\rm C}}(t)\rangle + \int_{-\infty}^{t} dt'G_0(t,t')V_{\rm S}|\Psi_{\mathbf{p},{\rm C}}(t')\rangle, \tag{10}$$

where $|\Psi_{\mathbf{p},{\rm C}}(t)\rangle = iG_{\rm C}(t,t')|\psi_{\rm in}(t')\rangle$, with $|\Phi_{\rm in}(t)\rangle = |\psi_{\rm in}(t)\rangle|0_{\mathbf{K}}\rangle$; i.e., the state $|\Psi_{\mathbf{p},{\rm C}}(t)\rangle$ evolves from the initial state of the electron under action of the Green's operator $G_{\rm C}$ that corresponds to the Hamiltonian $H_0 - V_{\rm S}$. We approximate $|\Psi_{\mathbf{p},{\rm C}}(t)\rangle$ by the Volkov wave vector in the length gauge

$$\begin{aligned} |\Psi_{\mathbf{p},{\rm C}}(t)\rangle &\approx |\chi_{\mathbf{p}}(t)\rangle \\ &= |\mathbf{p} + \mathbf{A}(t)\rangle\exp\{-i[\mathbf{p}\cdot\boldsymbol{\alpha}(t) + \mathcal{U}(t) + E_{\mathbf{p}}t]\}, \end{aligned} \tag{11}$$

where $\boldsymbol{\alpha}(t) = \int^t dt'\mathbf{A}(t')$, $E_{\mathbf{p}} = \mathbf{p}^2/2$, and

$$\mathcal{U}(t) = \frac{1}{2}\int^t dt'\mathbf{A}^2(t') = \mathcal{U}_1(t) + U_{\rm p}t,$$

with $\mathbf{E}_{\rm L}(t) = -d\mathbf{A}(t)/dt$, $U_{\rm p}$ the ponderomotive energy, and $\mathcal{U}_1(t)$ the time-periodic part of $\mathcal{U}(t)$. We also replace the Green's operator G_0 in Eq. (10) by the Volkov Green's operator

$$G_{\rm L}(t,t') = -i\theta(t-t')\int d^3\mathbf{q}|\chi_{\mathbf{q}}(t)\rangle\langle\chi_{\mathbf{q}}(t')|. \tag{12}$$

Finally, we neglect the field dressing of the final state $|\Phi_{\rm f}(t)\rangle$, describing it by the atomic ground state multiplied by the one-photon state of the x-ray field: $|\Phi_{\rm f}(t)\rangle \approx |\psi_{\rm B}\rangle\exp(-iE_{\rm B}t)|1_{\mathbf{K}}\rangle$, where $E_{\rm B}$ denotes the electron binding energy, i.e., the energy of the atomic bound state. We apply all these approximations to the S matrix (9). We also put $t \to 0$ and $t' \to T_{\rm p}$, instead of $t \to -\infty$ and $t' \to \infty$, in the limits of Eq. (9), since we want to analyze electron-ion recombination in a few-cycle laser pulse of duration $T_{\rm p}$ (the values $t \to -\infty$ and $t' \to \infty$ were used for

an infinitely long laser pulse). For the same reason, we put 0 instead of $-\infty$ in the lower limit of integral in Eq. (10). By combining Eqs. (9) and (10), modified in such a way, and introducing all the above-mentioned approximations, we get

$$S_{\rm fi} = -C_{\mathbf{K}} \int_0^{T_{\rm p}} dt\, e^{i(E_{\rm B}+\omega_{\mathbf{K}})t} \Big\{ \langle \psi_{\rm B}|\mathbf{r}\cdot\hat{\mathbf{e}}_{\mathbf{K}} e^{-i\mathbf{K}\cdot\mathbf{r}}|\chi_{\tilde{\mathbf{p}}}(t)\rangle - i\int_0^t dt' \int d^3\mathbf{q} \langle \psi_{\rm B}|\mathbf{r}\cdot\hat{\mathbf{e}}_{\mathbf{K}} e^{-i\mathbf{K}\cdot\mathbf{r}}|\chi_{\mathbf{q}}(t)\rangle \times \langle \chi_{\mathbf{q}}(t')|V_{\rm S}|\chi_{\tilde{\mathbf{p}}}(t')\rangle \Big\}, \tag{13}$$

where $\mathbf{q}$ is the intermediate electron momentum, while $\tilde{\mathbf{p}}$ in $\chi_{\tilde{\mathbf{p}}}$ denotes the shifted electron momentum, which is explained later. Further calculations are simple but long and we only mention the basic steps: The substitution $t' = t - \tau$ is used, so that the integral over the scattering times t' in Eq. (13) is replaced by an integral over the travel times τ (i.e., the times between the scattering and the recombination). This substitution makes it possible to solve the integral over intermediate electron momenta $\mathbf{q}$ by the saddle-point method [4,6,25,26]. The integral over $\mathbf{q}$ can generally be presented as a Taylor expansion around the saddle point $\mathbf{q} = \mathbf{k}_{\rm s}$ that contains powers of $1/\tau$ multiplied by the even derivatives of the subintegral function over the intermediate electron momenta. The main contribution comes from the zeroth-order term in the expansion and all other terms may be neglected. In our case, the final result (up to a phase factor) is

$$S_{\rm fi} \approx -C_{\mathbf{K}} \int_0^{T_{\rm p}} dt\, e^{i[(E_{\rm B}+\omega_{\mathbf{K}}-\tilde{E}_{\mathbf{p}}-U_{\rm p})t - \tilde{\mathbf{p}}\cdot\boldsymbol{\alpha}(t) - \mathcal{U}_{\rm I}(t)]} \times \Big\{ \langle \psi_{\rm B}|\mathbf{r}\cdot\hat{\mathbf{e}}_{\mathbf{K}} e^{-i\mathbf{K}\cdot\mathbf{r}}|\tilde{\mathbf{p}}+\mathbf{A}(t)\rangle - i\int_0^t d\tau \left(\frac{2\pi}{i\tau}\right)^{3/2} \times \langle \psi_{\rm B}|\mathbf{r}\cdot\hat{\mathbf{e}}_{\mathbf{K}} e^{-i\mathbf{K}\cdot\mathbf{r}}|\mathbf{k}_{\rm s}+\mathbf{A}(t)\rangle \langle \mathbf{k}_{\rm s}|V_{\rm S}|\tilde{\mathbf{p}}\rangle e^{i(\tilde{\mathbf{p}}-\mathbf{k}_{\rm s})^2\tau/2} \Big\}, \tag{14}$$

where $\tilde{E}_{\mathbf{p}} = \tilde{\mathbf{p}}^2/2$ and $\tilde{\mathbf{p}} \equiv \mathbf{p} - \mathbf{A}(0)$, while the stationary intermediate electron momentum is $\mathbf{k}_{\rm s} = [\boldsymbol{\alpha}(t-\tau) - \boldsymbol{\alpha}(t)]/\tau$. The shift of the incident electron momentum by $\mathbf{A}(0)$ is related to the fact that the vector potential $\mathbf{A}(t)$ may be different from zero at the beginning of the pulse, i.e., $\mathbf{A}(0) \neq \mathbf{0}$. The introduction of the shifted electron momentum $\tilde{\mathbf{p}}$ assures that we calculate the probability of transition from an incident electron state with the momentum $\mathbf{p}$ to an emitted photon state with the momentum $\mathbf{K}$ at the detector outside the laser field. This is a situation similar to the introduction of the final electron momentum shift in the above-threshold ionization by few-cycle pulses [27]. The shifted electron momenta were also introduced in Ref. [28], where few-cycle-laser-pulse-assisted electron-atom potential scattering was analyzed.

The first term on the right-hand side of Eq. (14), which is proportional to $\langle \psi_{\rm B}|\mathbf{r}\cdot\hat{\mathbf{e}}_{\mathbf{K}} e^{-i\mathbf{K}\cdot\mathbf{r}}|\tilde{\mathbf{p}}+\mathbf{A}(t)\rangle$, describes the process in which the electron, dressed by the few-cycle laser field, recombines with the positive ion. The recombination occurs at the time t and the integration is done over entire pulse duration, i.e., from $t = 0$ to $t = T_{\rm p}$. The above-mentioned first term provides a plateau in the photon energy spectrum. The second term on the right-hand side of Eq. (14) is the second Born approximation for the few-cycle-laser-pulse-assisted electron-ion recombination. It describes the process in which the electron first scatters off an ion at the time $t - \tau$, then moves in the laser field during the time from $t - \tau$ to t, and finally recombines with the same ion at the time t. The integration is done over all electron travel times τ from 0 to t and over all recombination times t from the beginning ($t = 0$) to the end ($t = T_{\rm p}$) of the pulse. The factor $\tau^{-3/2}$ comes from the saddle-point-method solution of the integral over all intermediate electron momenta $\mathbf{q}$ ($\mathbf{q} \to \mathbf{k}_{\rm s}$; see Appendix A in Ref. [29]). The second term is responsible for the appearance of another plateau in the energy spectrum. This second plateau is considerably lower than the first one and may be observed in the high-energy region of the recombination spectrum. It was first found in Ref. [12] (see also Refs. [14,15]) for an infinitely long pulse.

For the pulse defined by Eq. (2), we have $\boldsymbol{\alpha}(t) = \alpha(t)\hat{\mathbf{e}}_{\rm L}$ and $\mathbf{A}(t) = A(t)\hat{\mathbf{e}}_{\rm L}$, with

$$A(t) = -\frac{E_0}{2\omega}\left[\sin(\omega t+\phi) - \frac{1}{2}\sum_{j=1,2}\frac{\omega}{\omega_j}\sin(\omega_j t+\phi)\right] \tag{15}$$

and

$$\alpha(t) = \frac{E_0}{2\omega^2}\left[\cos(\omega t+\phi) - \frac{1}{2}\sum_{j=1,2}\left(\frac{\omega}{\omega_j}\right)^2\cos(\omega_j t+\phi)\right], \tag{16}$$

where $\omega_1 = \omega + \omega_{\rm p}$, $\omega_2 = \omega - \omega_{\rm p}$, $\omega_{\rm p} = \omega/n_{\rm p} = 2\pi/T_{\rm p}$, so that $A(t)$ and $\alpha(t)$ are time-periodic with the period $T_{\rm p}$. We calculate the spectra for the emitted x-ray energies that satisfy the relation

$$\omega_{\mathbf{K}} = \tilde{E}_{\mathbf{p}} + |E_{\rm B}| + U_{\rm p} + n\omega_{\rm p}, \tag{17}$$

with integer $n > -(\tilde{E}_{\mathbf{p}} + |E_{\rm B}| + U_{\rm p})/\omega_{\rm p}$. The differential rate for the electron-ion recombination assisted by a few-cycle laser pulse can be defined as the differential probability per unit time for the emission of an x-ray photon having the energy $\omega_{\mathbf{K}}$ into the solid-angle element $d\Omega_{\mathbf{K}}$, after the recombination of an electron having initial energy $E_{\mathbf{p}}$ and impinging from within the solid angle $d\Omega_{\mathbf{p}}$, multiplied by the energy interval $\omega_{\rm p}$ between the subsequent points in the energy spectrum [see Eq. (17)]. The result is

$$dw(\mathbf{K},\mathbf{p}) = \frac{p\omega_{\mathbf{K}}^3}{(2\pi)^2 c^3}\frac{|S_{\rm fi}|^2}{C_{\mathbf{K}}^2 T_{\rm p}}\omega_{\rm p} d\Omega_{\mathbf{K}} dE_{\mathbf{p}} d\Omega_{\mathbf{p}}. \tag{18}$$

We calculate the differential power spectrum

$$S(\mathbf{K},\mathbf{p}) = \frac{2\pi\omega_{\mathbf{K}} dw(\mathbf{K},\mathbf{p})}{d\Omega_{\mathbf{K}} dE_{\mathbf{p}} d\Omega_{\mathbf{p}}}, \tag{19}$$

where the factor 2π comes from the integration over the azimuthal angle of the incident electron momentum $\mathbf{p}$.

We model the short-range scattering potential by the double Yukawa potential

$$V_{\rm S}(r) = -\frac{Z}{H}\frac{e^{-r/D}}{r}[1 + (H-1)e^{-Hr/D}], \tag{20}$$

where $H = DZ^{0.4}$, Z is the nuclear charge, and the values of D for various atomic targets are given in Ref. [30].

III. CLASSICAL ANALYSIS

We now perform the classical analysis of the direct recombination and recombination after a scattering. To this end, we consider the arguments of the exponential functions in the first and second terms on the right-hand side of Eq. (14). The first term in Eq. (14) describes the direct recombination, and the corresponding argument of the exponential function is

$$S_1 = (E_B + \omega_K - \tilde{E}_p - U_p)t - \tilde{\mathbf{p}} \cdot \boldsymbol{\alpha}(t) - \mathcal{U}_1(t), \tag{21}$$

where t is the recombination time. The stationarity condition $\partial S_1/\partial t = 0$ gives

$$E_B + \omega_K - \frac{\tilde{\mathbf{p}}^2}{2} - \tilde{\mathbf{p}} \cdot \mathbf{A}(t) - \frac{\mathbf{A}^2(t)}{2} = 0, \tag{22}$$

which can be written in the form

$$\tfrac{1}{2}[\tilde{\mathbf{p}} + \mathbf{A}(t)]^2 = E_B + \omega_K. \tag{23}$$

This is the energy-conserving condition at the recombination time t; i.e., the kinetic energy of the incident electron in the laser field at time t must be equal to the sum of the electron binding energy E_B and the emitted x-ray energy ω_K. If $E_B + \omega_K < 0$ (this is possible because $E_B < 0$), Eq. (23) has complex solutions for the recombination time t. We only consider the case $E_B + \omega_K > 0$ for which Eq. (23) has real solutions for t. We write Eq. (23) in the form

$$\omega_K = \tfrac{1}{2}[\tilde{\mathbf{p}} + \mathbf{A}(t)]^2 - E_B \tag{24}$$

and calculate ω_K for specified values of t. In this way, we perform the classical analysis of the direct recombination.

The second term in Eq. (14) corresponds to the recombination with a previous scattering. The argument of the exponential function in the second term is

$$S_2 = (E_B + \omega_K - \tilde{E}_p - U_p)t - \tilde{\mathbf{p}} \cdot \boldsymbol{\alpha}(t) - \mathcal{U}_1(t) + \frac{\tau}{2}(\tilde{\mathbf{p}} - \mathbf{k}_s)^2, \tag{25}$$

where t is the recombination time and τ is the travel time. From the conditions $\partial S_2/\partial t = 0$ and $\partial S_2/\partial \tau = 0$ we get

$$\tilde{\mathbf{p}}^2 + 2(\tilde{\mathbf{p}} - \mathbf{k}_s) \cdot \mathbf{A}(t - \tau) - \mathbf{k}_s^2 = 0, \tag{26}$$

$$2(E_B + \omega_K) - \mathbf{k}_s^2 - 2\mathbf{k}_s \cdot \mathbf{A}(t) - \mathbf{A}^2(t) = 0. \tag{27}$$

Equations (26) and (27) can be rewritten as

$$\tfrac{1}{2}[\mathbf{k}_s + \mathbf{A}(t - \tau)]^2 = \tfrac{1}{2}[\tilde{\mathbf{p}} + \mathbf{A}(t - \tau)]^2, \tag{28}$$

$$E_B + \omega_K = \tfrac{1}{2}[\mathbf{k}_s + \mathbf{A}(t)]^2, \tag{29}$$

respectively. Equation (28) is the electron-energy-conserving condition at the scattering time $t - \tau$, while Eq. (29) expresses the energy-conserving condition at the recombination time t. Equations (28) and (29) represent a system of two nonlinear equations which can be solved numerically in order to calculate the emitted x-ray energy ω_K for different values of the travel time τ. Considering the fact that a large number of travel times may correspond to the same value of ω_K, we calculate only the maximum value of ω_K and its corresponding travel time τ.

IV. NUMERICAL RESULTS

In all our calculations, we assume that the laser field is linearly polarized with the electric field vector given by Eq. (2)

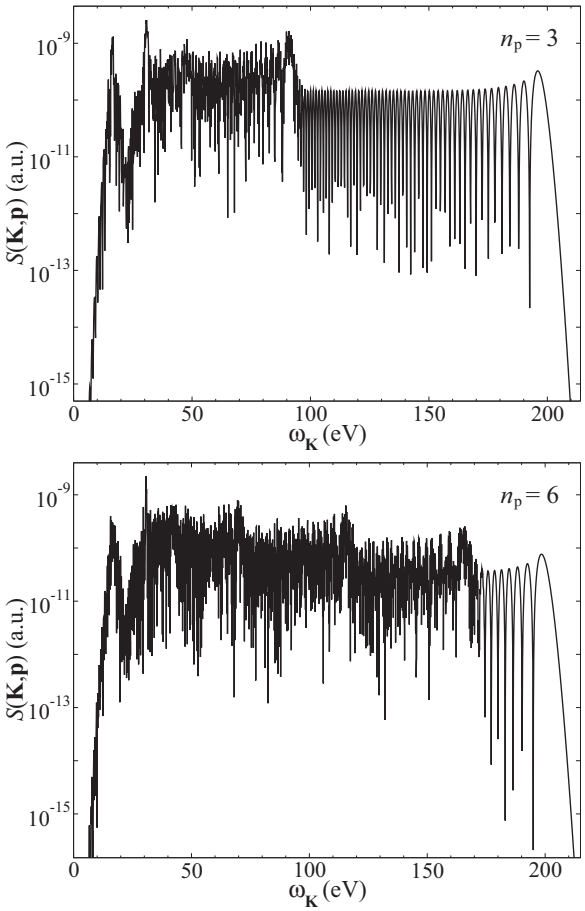

FIG. 1. The differential power spectrum for the laser-assisted radiative recombination of electrons with Ar^+ ions in the presence of a linearly polarized few-cycle laser pulse, as a function of the emitted x-ray energy ω_K. Only the direct recombination (LAR) is included. The laser pulse has a wavelength of 3200 nm and a peak intensity of 5×10^{13} W/cm^2, while the CEP is $\phi = 0°$. The incident electron energy is $E_p = 15$ eV and the incident electron angle is $\theta = 0°$. The number of optical cycles n_p is denoted in each panel.

and that the polarization vector of the emitted x rays $\hat{\mathbf{e}}_K$ is in the direction of the laser-field polarization vector $\hat{\mathbf{e}}_L$.

A. Direct recombination spectra

We first consider the direct recombination of electrons with ionic targets (LAR). This process is described by the first term on the right-hand side of Eq. (14). In Fig. 1 the differential power spectrum for the laser-assisted radiative recombination of electrons with Ar^+ ions is presented as a function of the emitted x-ray energy. The recombination occurs in a linearly polarized few-cycle laser pulse having a wavelength of 3200 nm and an intensity of 5×10^{13} W/cm^2. The CEP of the laser pulse is $\phi = 0°$, while the number of optical cycles n_p is denoted in each panel of Fig. 1. The incident electron energy is $E_p = 15$ eV and the incident electron angle is $\theta = 0°$. The energy spectra in Fig. 1 show a plateau with an abrupt cutoff. The low-energy part of the plateau contains a dense and irregular oscillatory structure, while the oscillations in the high-energy part of the plateau are regular and occur with an order of magnitude lower intensity. It is also clearly

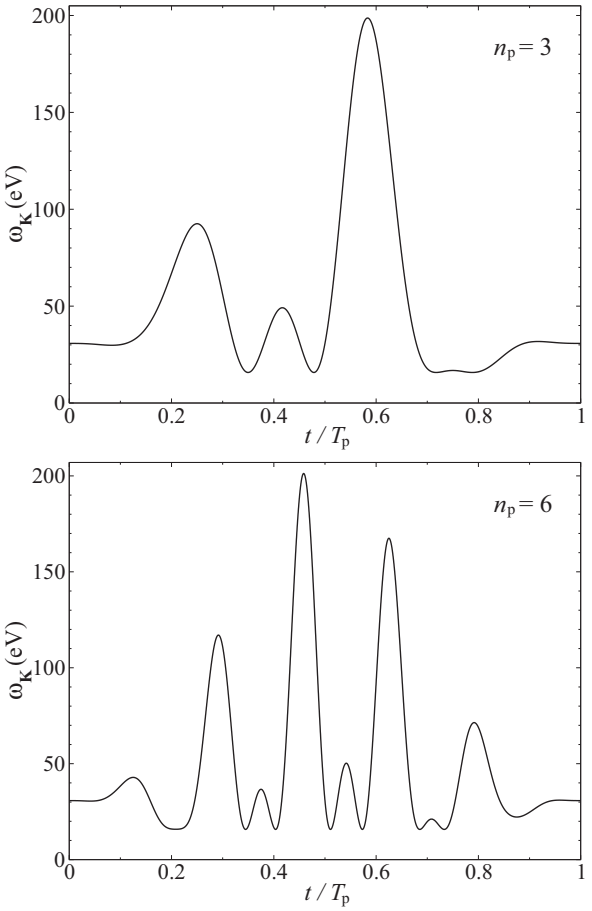

FIG. 2. Classical analysis of the direct recombination solutions for the parameters of Fig. 1. The emitted x-ray energy $\omega_{\mathbf{K}}$ is presented as a function of the recombination time t, expressed in laser-pulse duration time T_p. The number of optical cycles n_p is denoted in each panel.

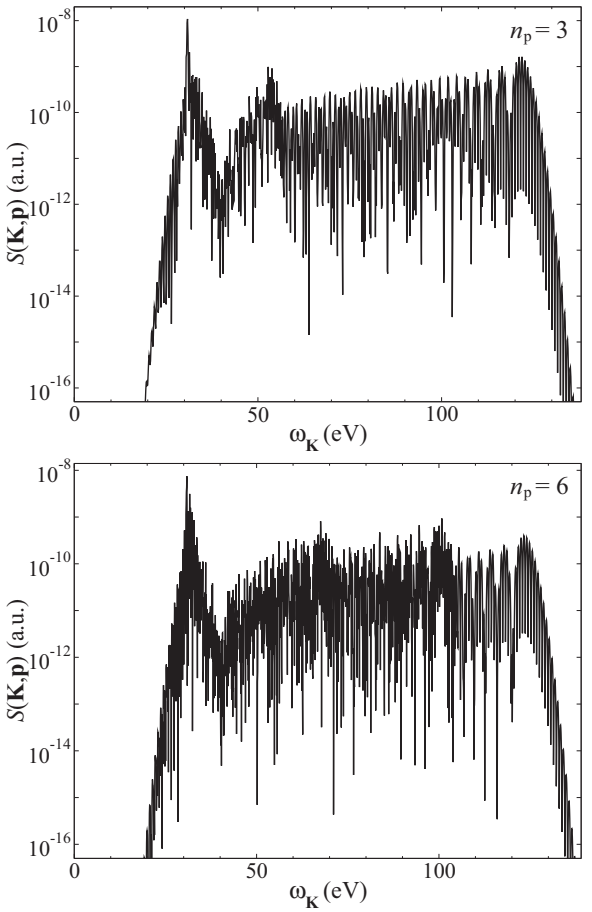

FIG. 3. Same as in Fig. 1, except that the incident electron angle is $\theta = 90^\circ$.

visible that the energy spectrum for six optical cycles is much richer with oscillations than that for three optical cycles. These oscillatory structures and cutoffs of the plateaus in energy spectra can be explained by the classical analysis of the direct recombination. Using Eq. (24) and setting all parameters the same as in Fig. 1, we have calculated the emitted x-ray energy $\omega_{\mathbf{K}}$ as a function of the recombination time t, expressed in units of T_p. The results are presented in Fig. 2, showing that more classical solutions, for a fixed value of $\omega_{\mathbf{K}}$, exist for $n_p = 6$ than for $n_p = 3$. While all solutions contribute to the process in the region of very low values of the emitted x-ray energy, the number of contributing solutions decreases with an increase of the emitted x-ray energy. In the region close to the plateau cutoff just one pair of solutions remains. The highest maximum in each panel of Fig. 2 matches the cutoff energy of the plateau in the corresponding panel of Fig. 1. By comparing Figs. 1 and 2, we conclude that the results obtained by numerical integration of the S matrix [Eqs. (14), (18), and (19)] agree very well with the estimates of the classical analysis [Eq. (24)].

Another example of the direct recombination energy spectrum is presented in Fig. 3. The incident electron angle is now $\theta = 90^\circ$, while the other parameters are the same as in Fig. 1. One can see from Fig. 3 that the oscillatory structure of the low-energy part of the spectrum is very similar to that in Fig. 1. However, the oscillations in the high-energy part of the spectrum are much richer and more irregular for $\theta = 90^\circ$ (Fig. 3) than those obtained for $\theta = 0^\circ$ (Fig. 1). The results of classical analysis, which are presented in Fig. 4, offer an explanation. Figure 4 shows two high-energy maxima (instead of one) in each panel, so that two pairs of classical solutions exist for the high values of the emitted x-ray energy (i.e., in the energy region close to the plateau cutoff). The interference of these four solutions produces rich oscillations in the high-energy part of the spectrum, near the plateau cutoff, as illustrated in Fig. 3. For $\theta = 0^\circ$, only two classical solutions exist for high values of the emitted x-ray energy near the cutoff value (see Fig. 2), which is the reason why the oscillations in the high-energy part of the plateau are less intense (see Fig. 1). A closer look at each panel of Fig. 4 shows that there is more than one pair of maxima that are identical in height and shape, and symmetrical in the recombination time t. More precisely, there are two such pairs of maxima for $n_p = 3$ and four for $n_p = 6$.

Let us explain the connection between the energy spectra obtained by numerical integration of the S-matrix element and the classical analysis. Instead of numerical integration over the time t in Eq. (14), the stationary phase method can be used in order to express the S-matrix element as a sum over the stationary points t_s [31]. For a given value of the emitted x-ray energy, there is a certain number of stationary

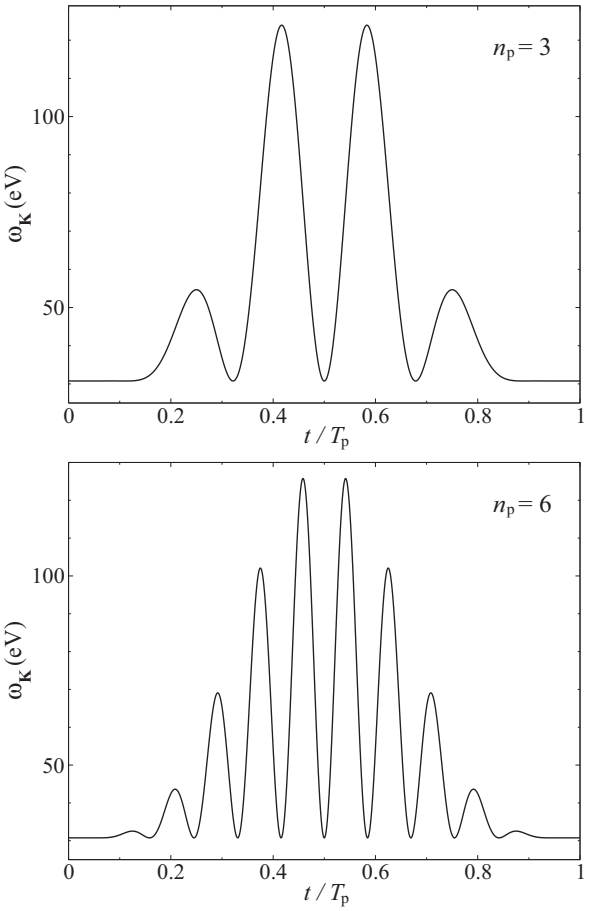

FIG. 4. Classical analysis of the direct recombination solutions for the parameters of Fig. 3. The notation is the same as in Fig. 2.

points t_s, i.e., the stationary phase solutions. Each of these stationary points gives a contribution to the S-matrix element. These contributions interfere, producing the oscillations in the energy spectrum. This oscillatory structure should be understood in terms of Feynman's path integral interpretation of quantum physics [32]: The probability amplitude of a quantum-mechanical process can be represented as a coherent superposition of all possible spatiotemporal paths that connect the initial and the final state of the system [33]. The interference of more contributions of the stationary points leads to a richer oscillatory structure of the energy spectrum. The stationary points are actually the recombination time solutions t for a given value of the emitted x-ray energy $\omega_{\mathbf{K}}$, as presented in Figs. 2 and 4. For example, let us consider the $n_p = 3$ case shown in the upper panel of Fig. 4. For fixed 30.8 eV$< \omega_{\mathbf{K}} <$ 54.7 eV, there are eight recombination time solutions (i.e., eight stationary points). This means that we have eight contributions to the S-matrix element for 30.8 eV$< \omega_{\mathbf{K}} <$ 54.7 eV. These contributions interfere, producing a dense oscillatory structure in the low-energy part of the spectrum (see the upper panel of Fig. 3). By looking at the upper panel of Fig. 4, one can also notice that there are only four recombination time solutions for 54.7 eV$< \omega_{\mathbf{K}} <$ 123.9 eV, so that only four contributions to the S-matrix element exist. This explains why the oscillations in this part of the energy spectrum are less pronounced than those observed for 30.8 eV$< \omega_{\mathbf{K}} <$ 54.7 eV, as one can see from the upper panel of Fig. 3. For $\omega_{\mathbf{K}} >$ 123.9 eV, no recombination time solution exists (see the upper panel of Fig. 4) and there is no contribution to the S-matrix element. The plateau in the energy spectrum ends with an abrupt cutoff when $\omega_{\mathbf{K}}$ increases over 123.9 eV (see the upper panel of Fig. 3). The connection between the energy spectrum and the recombination time solutions for $n_p = 6$ (the lower panels of Figs. 3 and 4) can be explained using the same arguments. The only difference is that we now have more recombination time solutions, i.e., more contributions to the S-matrix element. This results in a much richer and more irregular oscillatory structure of the energy spectrum, particularly in the low-energy part of the spectrum. The same line of reasoning can be applied to Figs. 1 and 2, where the numerical results and classical solutions for $\theta = 0^\circ$ are presented.

B. Spectra which include both the direct recombination and recombination with scattering

We now analyze the laser-assisted electron-ion radiative recombination with a previous scattering (SLAR). In order to include the scattering effects in our analysis, we take both terms on the right-hand side of Eq. (14) into account. We first illustrate the influence of the incident electron angle θ on the energy spectra. The results are shown in Fig. 5, where the differential power spectrum for the laser-assisted radiative recombination of electrons with He^+ ions is presented as a function of the emitted x-ray energy. The wavelength and peak intensity of the few-cycle laser pulse are 3500 nm and 2.5×10^{13} W/cm^2, respectively. The CEP of the pulse is $\phi = 0^\circ$ and the number of optical cycles is $n_p = 4$. The incident electron energy is $E_{\mathbf{p}} = 6$ eV and the incident electron angle θ is denoted in each panel of Fig. 5. The results presented in Fig. 5 clearly show that the plateau structures in energy spectra are strongly dependent on the incident electron angle. For $\theta = 0^\circ$ and $\theta = 30^\circ$, both the low- and high-energy parts of the plateau are qualitatively similar to that of Fig. 1. This plateau is a consequence of the direct recombination of electrons with ionic targets (LAR). For $\theta = 90^\circ$, the high-energy part of the LAR plateau becomes shorter, i.e., its cutoff is shifted to lower energies (from 123.7 eV for $\theta = 0^\circ$ to 87.0 eV for $\theta = 90^\circ$). However, for $\theta = 90^\circ$, a new high-energy plateau emerges. This second plateau extends up to 114.9 eV and is seven to eight orders of magnitude lower than the first one. It represents the contribution of the laser-assisted electron-ion recombination with a previous scattering (SLAR) to the energy spectrum. We have checked this by calculating separately the contributions of the LAR and SLAR processes to the spectrum. If the angle is increased from $\theta = 0^\circ$ to $\theta = 90^\circ$, the cutoff energy of the first plateau decreases and this plateau becomes shorter. At a certain value of the angle θ, the second plateau, which is seven to eight orders of magnitude lower, becomes visible in the spectrum. A further increase of the angle θ beyond 90° causes an increase of the cutoff energy of the first plateau and this plateau becomes longer. For large values of the incident electron angle, the first (higher) plateau once again becomes longer than the second (lower) one, so that the SLAR effects are again masked by the LAR contribution. This behavior of the plateaus in the energy spectrum is confirmed

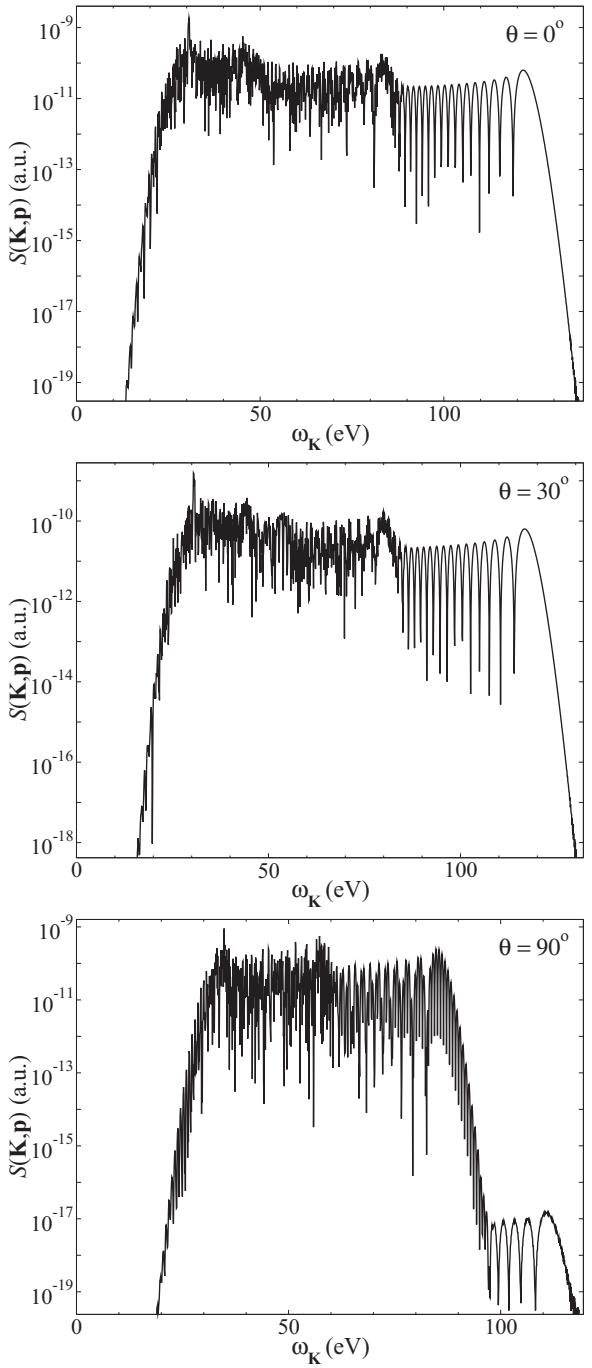

FIG. 5. The differential power spectrum for the laser-assisted radiative recombination of electrons with He^+ ions in the presence of a linearly polarized few-cycle laser pulse, as a function of the emitted x-ray energy $\omega_{\mathbf{K}}$. Both the LAR and SLAR processes are included. The laser pulse has a wavelength of 3500 nm and a peak intensity of 2.5×10^{13} W/cm^2. The CEP of the pulse is $\phi = 0^\circ$ and the number of optical cycles is $n_p = 4$. The incident electron energy is $E_{\mathbf{p}} = 6$ eV, while the incident electron angle θ is denoted in each panel.

by our classical analysis, the results of which are illustrated in Fig. 6, where the maximum value of the emitted x-ray energy is presented as a function of the angle θ. One can conclude that the best chance to observe the SLAR effects (i.e., the second plateau) is at $\theta = 90^\circ$.

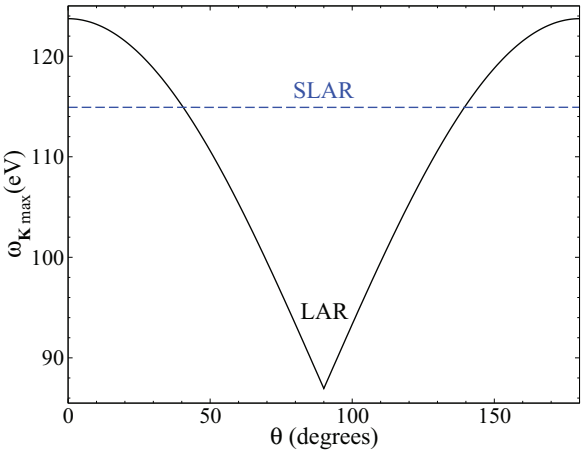

FIG. 6. (Color online) Classical results for the maximum value of the emitted x-ray energy in the electron–He^+-ion radiative recombination process as a function of the incident electron angle θ. The laser field parameters and the incident electron energy are the same as in Fig. 5. The results for LAR (solid black line) and SLAR (dashed blue line) are presented.

Let us now consider the influence of the CEP ϕ on the energy spectra. The results are shown in Fig. 7, where the differential power spectrum for the laser-assisted radiative recombination of electrons with He^+ ions is presented as a function of the emitted x-ray energy. The process is assisted by a linearly polarized few-cycle laser pulse having a wavelength of 3700 nm and an intensity of 3×10^{13} W/cm^2, while the number of optical cycles is $n_p = 4$. The value of the CEP ϕ is denoted in each panel of Fig. 7. The incident electron energy and angle are $E_{\mathbf{p}} = 5$ eV and $\theta = 90^\circ$, respectively. There are two plateaus in each panel of Fig. 7. As noted above, the first (higher) plateau is a consequence of LAR, while the second plateau, which is seven orders of magnitude lower, describes SLAR. One can notice that a change of the CEP affects the oscillatory structure of the energy spectrum and it also shifts the cutoff positions of the plateaus. Using the classical analysis of the LAR and SLAR, we can predict how the cutoff energy for the LAR and SLAR depends on the CEP. The results are shown in Fig. 8, where the maximum value of the emitted x-ray energy is presented as a function of the CEP.

The plateaus in the energy spectrum of the laser-assisted electron-ion recombination are also sensitive to the incident electron energy. This is illustrated in Fig. 9, where the differential power spectrum for the laser-assisted radiative recombination of electrons with He^+ ions is presented as a function of the emitted x-ray energy. The process occurs in a linearly polarized few-cycle laser pulse having a wavelength of 3300 nm and an intensity of 6×10^{13} W/cm^2. The CEP of the laser pulse is $\phi = 0^\circ$, while the number of optical cycles is $n_p = 4$. The incident electron angle is $\theta = 90^\circ$. The energy of the incident electrons varies from 10 to 60 eV. As the incident electron energy increases, the entire LAR plateau shifts to higher energies; i.e., both the minimum and maximum values of the emitted x-ray energy increase. At low incident electron energies, the SLAR plateau, which is seven to eight orders of magnitude lower than the LAR plateau, can be observed in the high-energy part of the spectrum, as

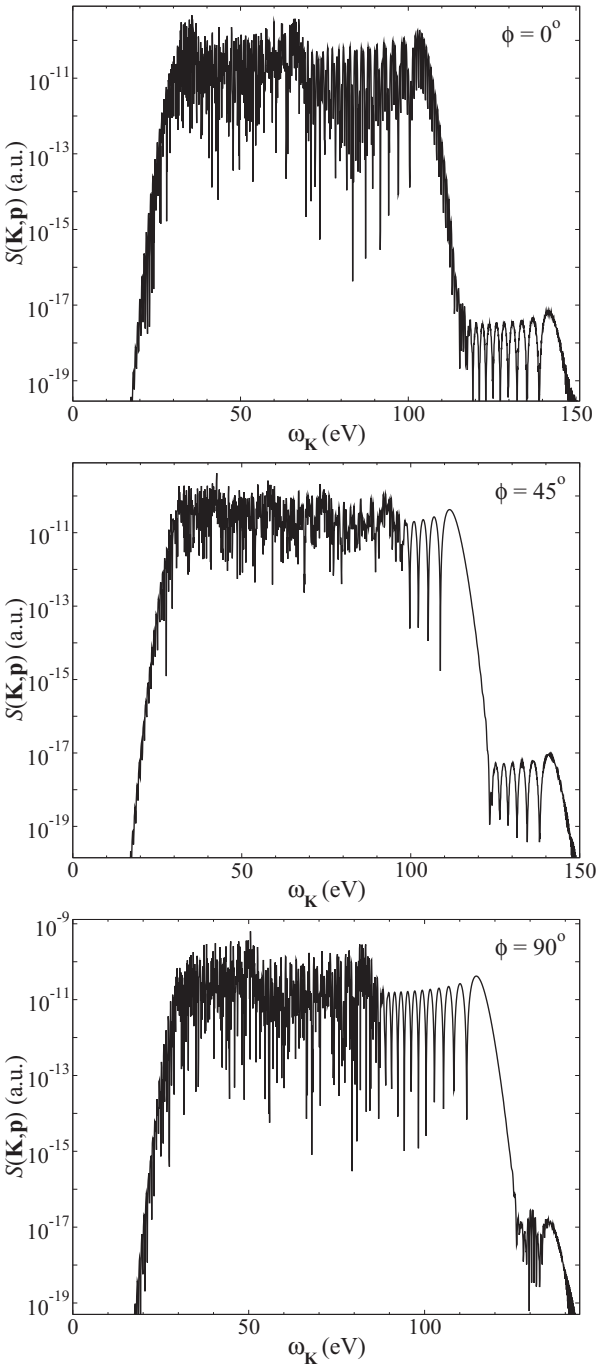

FIG. 7. The differential power spectrum for the laser-assisted radiative recombination of electrons with He^+ ions in the presence of a linearly polarized few-cycle laser pulse, as a function of the emitted x-ray energy $\omega_{\mathbf{K}}$. Both the direct recombination (LAR) and recombination with a previous scattering (SLAR) are included. The laser wavelength and peak intensity are 3700 nm and 3×10^{13} W/cm^2, respectively, while the number of optical cycles is $n_p = 4$. The incident electron energy is $E_{\mathbf{p}} = 5$ eV and the incident electron angle is $\theta = 90^\circ$. The CEP ϕ is denoted in each panel.

one can see from the top panel of Fig. 9, where the results for $E_{\mathbf{p}} = 10$ eV are presented. An increase of the incident electron energy causes a shift of the LAR plateau to higher energies in the spectrum, so that the low-energy part of the

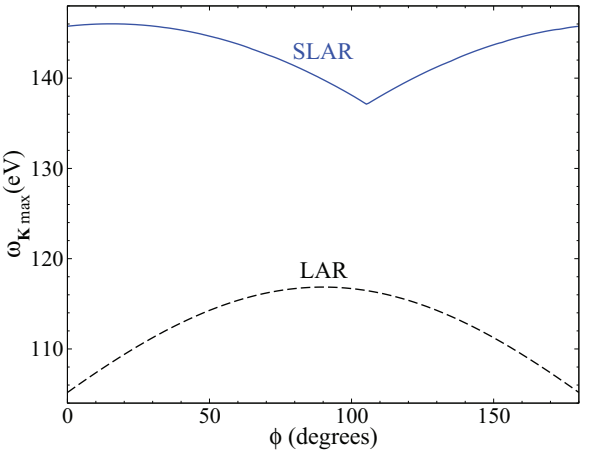

FIG. 8. (Color online) Classical results for the maximum value of the emitted x-ray energy in the electron–He^+-ion radiative recombination process as a function of the CEP ϕ. The other laser-field parameters and the incident electron energy and angle are the same as in Fig. 7. The results for LAR (dashed black line) and SLAR (solid blue line) are presented.

SLAR plateau becomes visible. This can be seen from the middle panel of Fig. 9, where the results for $E_{\mathbf{p}} = 30$ eV are presented. The low-energy part of the SLAR plateau is visible for the x-ray energies between 25 and 45 eV and its height is in the region from 10^{-17} to 10^{-15} a.u. Finally, if the incident electron energy is high enough, the high-energy part of the SLAR plateau is completely masked by the much higher LAR plateau, so that only the low-energy part of the SLAR plateau can be observed. Such a case is shown in the bottom panel of Fig. 9, where the results for $E_{\mathbf{p}} = 60$ eV are presented and the SLAR plateau appears in the low-energy region between 25 and 70 eV. We also notice from Fig. 9 that the low-energy part of the SLAR plateau is higher by one or two orders of magnitude than the high-energy part of the same plateau [compare the spectrum in the region 25–45 eV with that in the region 190–200 eV in Fig. 9(b)].

The dependence of the plateau structures on the laser pulse intensity is shown in Fig. 10, where the differential power spectrum for the laser-assisted radiative recombination of electrons with He^+ ions is presented as a function of the emitted x-ray energy. The laser wavelength is 3600 nm, the CEP of the pulse is $\phi = 0^\circ$ and the number of optical cycles is $n_p = 4$. The incident electron energy is $E_{\mathbf{p}} = 10$ eV, while the incident electron angle is $\theta = 90^\circ$. The results for two different peak intensities of the laser pulse are presented. At lower intensities of the laser pulse, only the LAR plateau can be observed in the energy spectrum. Such an example is shown in the upper panel of Fig. 10, where the results for $I = 10^{13}$ W/cm^2 are presented. With the increase of the laser pulse intensity, the SLAR plateau appears in the high-energy part of the spectrum, as one can see from the lower panel of Fig. 10, where the results for $I = 5 \times 10^{13}$ W/cm^2 are presented. Comparing the results in the upper and lower panels of Fig. 10, we conclude that the cutoff energy (i.e., the maximum energy of the emitted x rays) of the both plateaus increases with the increase of the laser pulse intensity. We also note that the cutoff energy of the SLAR plateau increases faster than that of the

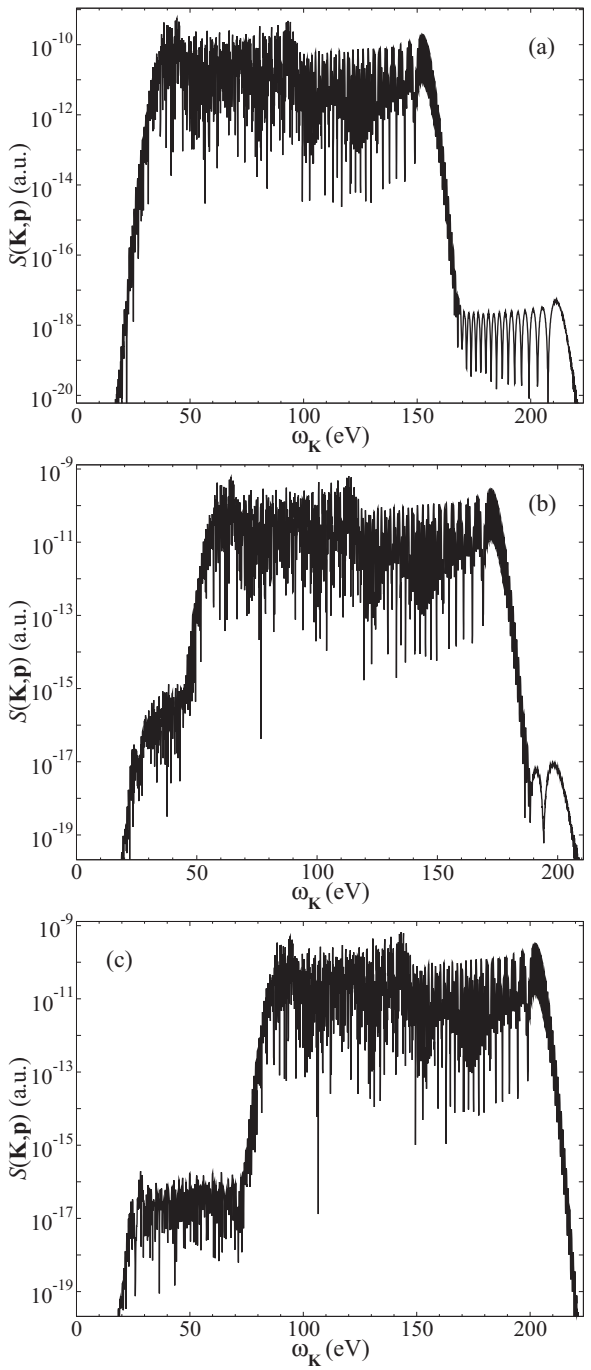

FIG. 9. The differential power spectrum for the laser-assisted radiative recombination of electrons with He^+ ions in the presence of a linearly polarized few-cycle laser pulse, as a function of the emitted x-ray energy $\omega_{\mathbf{K}}$. Both the direct recombination (LAR) and recombination with a previous scattering (SLAR) are included. The laser wavelength and peak intensity are 3300 nm and 6×10^{13} W/cm^2, respectively. The CEP of the pulse is $\phi = 0^\circ$ and the number of optical cycles is $n_p = 4$. The incident electron angle is $\theta = 90^\circ$, while the incident electron energies are (a) $E_{\mathbf{p}} = 10$ eV, (b) $E_{\mathbf{p}} = 30$ eV, and (c) $E_{\mathbf{p}} = 60$ eV.

LAR plateau, so that the SLAR plateau appears in the energy spectrum at a certain value of the laser pulse intensity.

We now consider how the number of optical cycles of the laser pulse affects the energy spectrum of electron-ion

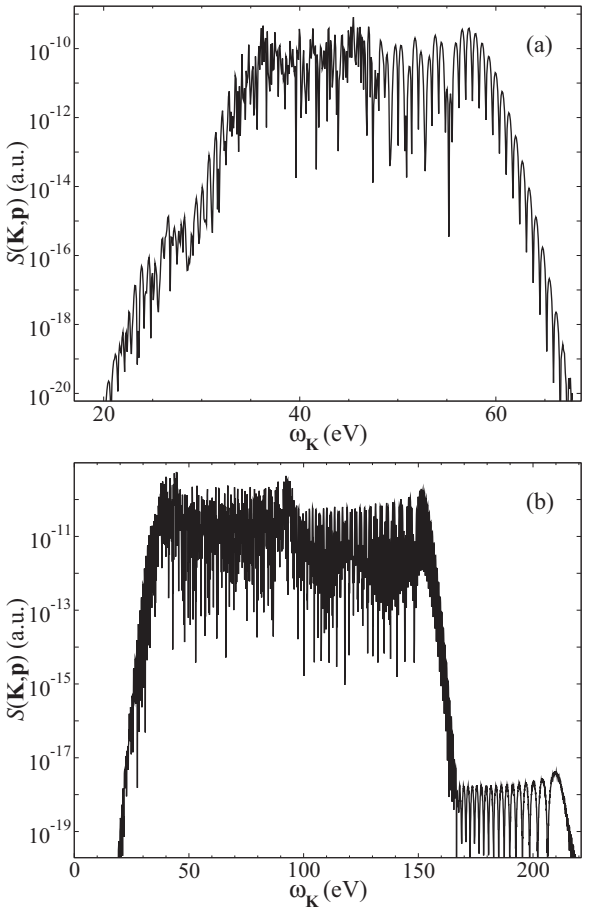

FIG. 10. The differential power spectrum for the laser-assisted radiative recombination of electrons with He^+ ions in the presence of a linearly polarized few-cycle laser pulse, as a function of the emitted x-ray energy $\omega_{\mathbf{K}}$. Both the direct recombination (LAR) and recombination with a previous scattering (SLAR) are included. The laser wavelength is 3600 nm, the CEP of the pulse is $\phi = 0^\circ$, and the number of optical cycles is $n_p = 4$. The incident electron energy and angle are $E_{\mathbf{p}} = 10$ eV and $\theta = 90^\circ$, respectively. The peak intensities of the laser pulse are (a) 10^{13} W/cm^2 and (b) 5×10^{13} W/cm^2.

radiative recombination when scattering effects are included. In Fig. 11 the differential power spectrum for the laser-assisted radiative recombination of electrons with He^+ ions is presented as a function of the emitted x-ray energy. The wavelength and peak intensity of the few-cycle laser pulse are 3400 nm and 4×10^{13} W/cm^2, respectively. The CEP of the pulse is $\phi = 0^\circ$, while the number of optical cycles n_p is denoted in each panel of Fig. 11. The incident electron energy and angle are $E_{\mathbf{p}} = 7$ eV and $\theta = 90^\circ$, respectively. When we have previously considered the LAR process, we have seen that the oscillations in the energy spectrum were denser and more pronounced for the greater number of optical cycles (the energy spectra for $n_p = 3$ and $n_p = 6$ were compared). The same is true for the SLAR process, as we can see from Fig. 11 where the energy spectra for $n_p = 4$ and $n_p = 7$ are presented (compare the corresponding SLAR plateaus which are visible in the region from 130 to 160 eV). Figure 11 shows that both the LAR and the SLAR plateau contain a richer and more irregular oscillatory structure for a larger number of optical

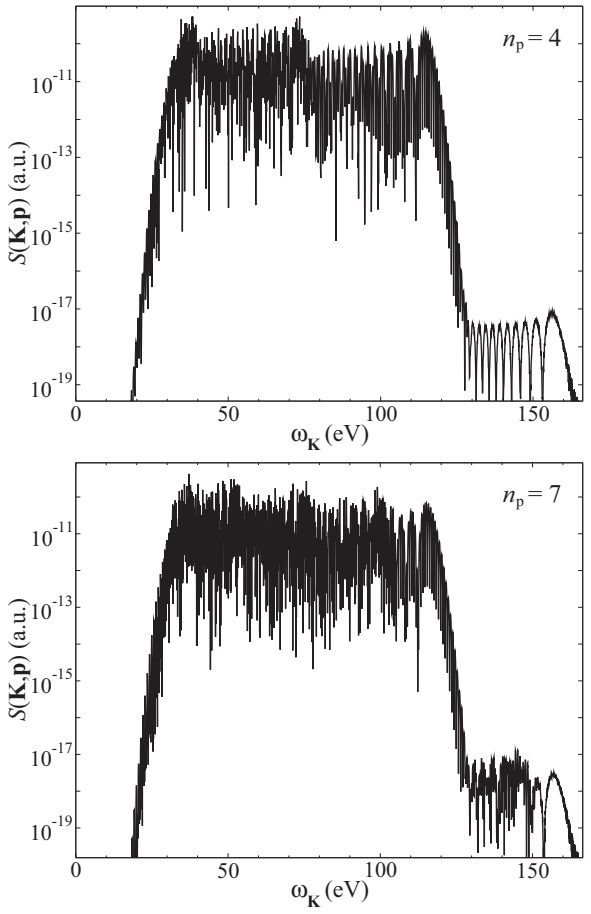

FIG. 11. The differential power spectrum for the laser-assisted radiative recombination of electrons with He^+ ions in the presence of a linearly polarized few-cycle laser pulse, as a function of the emitted x-ray energy $\omega_\mathbf{K}$. Both the LAR and SLAR are included. The laser wavelength and peak intensity are 3400 nm and 4×10^{13} W/cm^2, respectively, while the CEP is $\phi = 0^\circ$. The incident electron energy is $E_\mathbf{p} = 7$ eV and the incident electron angle is $\theta = 90^\circ$. The number of optical cycles n_p is denoted in each panel.

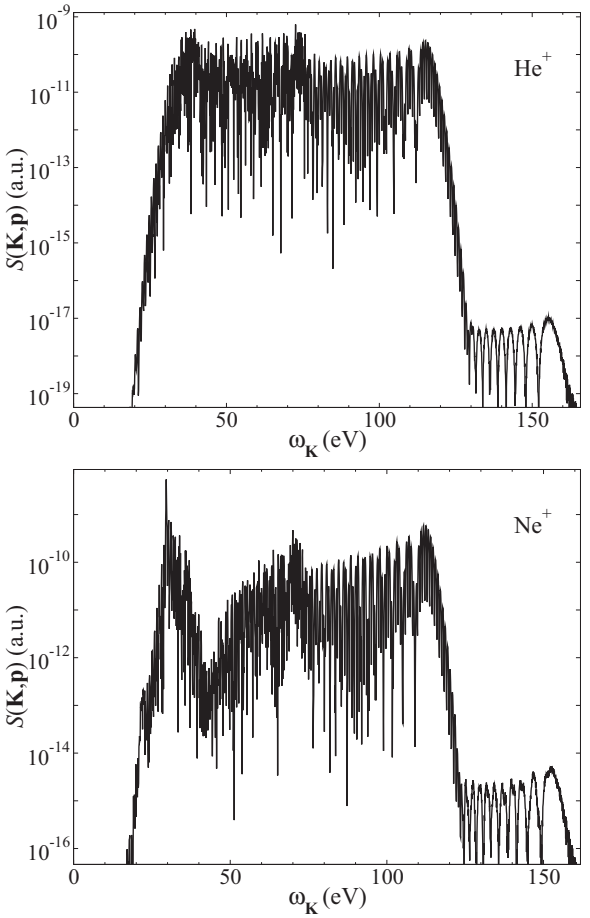

FIG. 12. The differential power spectrum for the laser-assisted radiative recombination of electrons with He^+(upper panel) and Ne^+(lower panel) ions in the presence of a linearly polarized few-cycle laser pulse, as a function of the emitted x-ray energy $\omega_\mathbf{K}$. Both the LAR and SLAR are included. The laser pulse has a wavelength of 3200 nm and a peak intensity of 4.5×10^{13} W/cm^2. The CEP of the pulse is $\phi = 0^\circ$ and the number of optical cycles is $n_p = 4$. The incident electron energy and angle are $E_\mathbf{p} = 8$ eV and $\theta = 90^\circ$, respectively.

cycles, i.e., for $n_p = 7$. This can be explained by the fact that the number of classical solutions for LAR and SLAR increases with the increase of n_p. We have illustrated this fact for LAR (see Figs. 2 and 4).

The type of the ionic target slightly affects the maximum value of the emitted x-ray energy for LAR and SLAR, due to the fact that different ions have different values of binding energy. On the other hand, the type of the ionic target strongly affects the value of the differential power spectrum. This is illustrated in Fig. 12, where the differential power spectrum for the laser-assisted radiative recombination of electrons with He^+ (upper panel) and Ne^+ (lower panel) ions is presented as a function of the emitted x-ray energy. The wavelength and peak intensity of the few-cycle laser pulse are 3200 nm and 4.5×10^{13} W/cm^2, respectively. The CEP of the pulse is $\phi = 0^\circ$, while the number of optical cycles is $n_p = 4$. The incident electron energy is $E_\mathbf{p} = 8$ eV and the incident electron angle is $\theta = 90^\circ$. Figure 12 shows that, while the cutoff positions of the LAR and SLAR plateau are only slightly different for He^+ and Ne^+, the differential power spectrum in the high-energy part of the spectrum is much larger for the electron–Ne^+-ion recombination than for the electron–He^+-ion recombination. Although the difference is small for LAR (first plateau), it is quite significant for SLAR (second plateau; almost three orders of magnitude). Therefore, we conclude that the process can be enhanced by the use of heavier ionic targets.

V. CONCLUSIONS

The laser-assisted electron-ion recombination belongs to less investigated processes in a strong laser field, both theoretically and experimentally. The experimental findings are scarce while the theoretical investigations are usually limited to the first-order process. The LAR process is a part (the third step) of the HHG process and is characterized by the femtosecond time scale. Recent experimental realization of few-cycle strong laser pulses in the mid-infrared region [34] and important results of their application to (i) inelastic

scattering of broadband electron wave packets driven by an intense mid-infrared laser field [35], (ii) generation of high-order harmonics of the order 5000 [36], and (iii) mid-infrared laser-induced electron diffraction, which is important for femtosecond molecular imaging [37,38], have stimulated us to explore the laser-assisted electron-ion recombination using few-cycle mid-infrared laser pulses.

We have formulated the S-matrix theory of few-cycle-laser-pulse-assisted electron-ion recombination. As in the case of an infinitely long flat pulse, in the few-cycle pulse case two plateaus appear in the energy spectra of the emitted x rays. The second plateau, which is due to SLAR process [12–15], is now investigated for few-cycle pulses. We have shown that the length of these plateaus depends on the value of CEP so that the cutoff position can be controlled changing the CEP, and, vice versa, the measurement of the cutoff position can be used to determine the value of CEP.

We have also investigated how the structure of the (S)LAR spectra depends on the laser pulse duration. We have concluded that the energy spectrum is characterized by the regions of intense oscillations and that the strength of these oscillations is higher for longer pulses. Our classical analysis has shown that the reason for such oscillatory behavior is the interference of a large number of quantum orbits [27,31,32]. For shorter pulses (consisting of three or four optical cycles) the number of such (classical) solutions is smaller and intense oscillations appear only for low energies of the emitted x-ray photons.

While analyzing the dependence of the spectra on the incident electron energy and angle, we have observed that the lower plateau, which is a consequence of the scattering (SLAR), appears also in the low-energy part (i.e., not only in the high-energy part) of the spectrum for certain values of the incident electron angle (close to $\theta = 90^\circ$) and for high incident electron energies.

For simulation of real experiments the recombination spectra should be averaged over the space-time distribution of laser intensity in focus. Such focal-averaged recombination spectra were calculated in Ref. [39]. In comparison with the fixed intensity spectra, shown in the present paper, the plateaus in the focal-averaged spectra [39] are more inclined and the oscillatory structure is suppressed (or even absent).

ACKNOWLEDGMENTS

Sponsorship has been provided by the Alexander von Humboldt Foundation and funding by the German Federal Ministry of Education and Research in the framework of the Research Group Linkage Programme.

[1] P. Salières, A. L'Huilier, Ph. Antoine, and M. Lewenstein, Adv. At. Mol. Opt. Phys. **41**, 83 (1999).
[2] T. Brabec and F. Krausz, Rev. Mod. Phys. **72**, 545 (2000).
[3] F. Ehlotzky, A. Jaroń, and J. Z. Kamiński, Phys. Rep. **297**, 63 (1998).
[4] D. B. Milošević and F. Ehlotzky, Phys. Rev. A **58**, 2319 (1998).
[5] D. B. Milošević and A. F. Starace, Phys. Rev. Lett. **81**, 5097 (1998); Laser Phys. **10**, 278 (2000).
[6] D. B. Milošević and A. F. Starace, J. Phys. B **32**, 1831 (1999); Phys. Rev. A **60**, 3943 (1999).
[7] A. Jaroń, J. Z. Kamiński, and F. Ehlotzky, Phys. Rev. A **61**, 023404 (2000); **63**, 055401 (2001); Laser Phys. **11**, 174 (2001); J. Phys. B **34**, 1221 (2001).
[8] M. Yu. Kuchiev and V. N. Ostrovsky, Phys. Rev. A **61**, 033414 (2000); J. Phys. B **34**, 405 (2001) (see the Appendix B about LAR in the context of HHG).
[9] D. B. Milošević and F. Ehlotzky, Adv. At. Mol. Opt. Phys. **49**, 373 (2003).
[10] C. Leone, S. Bivona, R. Burlon, and G. Ferrante, Phys. Rev. A **66**, 051403 (2002).
[11] G. Shchedrin and A. Volberg, J. Phys. A **44**, 245301 (2011).
[12] D. B. Milošević and F. Ehlotzky, Phys. Rev. A **65**, 042504 (2002).
[13] D. B. Milošević and F. Ehlotzky, J. Mod. Opt. **50**, 657 (2003).
[14] A. N. Zheltukhin, N. L. Manakov, A. V. Flegel, and M. V. Frolov, Pis'ma Zh. Eksp. Teor. Fiz. **94**, 641 (2011) [JETP Lett. **94**, 599 (2011)].
[15] A. N. Zheltukhin, A. V. Flegel, M. V. Frolov, N. L. Manakov, and A. F. Starace, J. Phys. B **45**, 081001 (2012).
[16] J. Z. Kamiński and F. Ehlotzky, Phys. Rev. A **71**, 043402 (2005); J. Mod. Opt. **53**, 7 (2006).
[17] S. Bivona, R. Burlon, G. Ferrante, and C. Leone, Opt. Express **14**, 3715 (2006).
[18] S. Bivona, R. Burlon, and C. Leone, Laser Phys. Lett. **4**, 44 (2007).
[19] K. R. Overstreet, R. R. Jones, and T. F. Gallagher, Phys. Rev. Lett. **106**, 033002 (2011).
[20] T. Mohamed, G. Andler, M. Fogle, E. Justiniano, S. Madzunkov, and R. Schuch, Phys. Rev. A **83**, 032702 (2011).
[21] T. Morishita, A. T. Le, Z. Chen, and C. D. Lin, Phys. Rev. Lett. **100**, 013903 (2008).
[22] M. V. Frolov, N. L. Manakov, T. S. Sarantseva, and A. F. Starace, Phys. Rev. A **83**, 043416 (2011).
[23] S. Minemoto, T. Umegaki, Y. Oguchi, T. Morishita, A. T. Le, S. Watanabe, and H. Sakai, Phys. Rev. A **78**, 061402(R) (2008).
[24] H. J. Wörner, H. Niikura, J. B. Bertrand, P. B. Corkum, and D. M. Villeneuve, Phys. Rev. Lett. **102**, 103901 (2009).
[25] D. B. Milošević and F. Ehlotzky, Phys. Rev. A **57**, 5002 (1998).
[26] D. B. Milošević and F. Ehlotzky, Phys. Rev. A **58**, 3124 (1998); J. Phys. B **31**, 4149 (1998); **32**, 1585 (1999).
[27] D. B. Milošević, G. G. Paulus, D. Bauer, and W. Becker, J. Phys. B **39**, R203 (2006).
[28] A. Čerkić and D. B. Milošević, Phys. Rev. A **87**, 033417 (2013).
[29] A. Gazibegović-Busuladžić, D. B. Milošević, and W. Becker, Phys. Rev. A **70**, 053403 (2004).
[30] A. E. S. Green, D. L. Sellin, and A. S. Zachor, Phys. Rev. **184**, 1 (1969).
[31] A. Čerkić and D. B. Milošević, Phys. Rev. A **73**, 033413 (2006).
[32] P. Salières, B. Carré, L. Le Déroff, F. Grasbon, G. G. Paulus, H. Walther, R. Kopold, W. Becker, D. B. Milošević, A. Sanpera, and M. Lewenstein, Science **292**, 902 (2001).
[33] D. B. Milošević, D. Bauer, and W. Becker, J. Mod. Opt. **53**, 125 (2006).

[34] O. D. Mücke, S. Ališauskas, A. J. Verhoef, A. Pugžlys, A. Baltuška, V. Smilgevičius, J. Pocius, L. Giniūnas, R. Danielius, and N. Forget, in *Advances in Solid-State Lasers: Development and Applications*, edited by M. Grishin (InTech, Croatia, 2010), p. 279.

[35] A. D. DiChiara, E. Sistrunk, C. I. Blaga, U. B. Szafruga, P. Agostini, and L. F. DiMauro, Phys. Rev. Lett. **108**, 033002 (2012).

[36] T. Popmintchev, M.-C. Chen, D. Popmintchev, P. Arpin, S. Brown, S. Ališauskas, G. Andriukaitis, T. Balčiunas, O. D. Mücke, A. Pugzlys, A. Baltuška, B. Shim, S. E. Schrauth, A. Gaeta, C. Hernández-García, L. Plaja, A. Becker, A. Jaron-Becker, M. M. Murnane, and H. C. Kapteyn, Science **336**, 1287 (2012).

[37] C. I. Blaga, J. Xu, A. D. DiChiara, E. Sistrunk, K. Zhang, P. Agostini, T. A. Miller, L. F. DiMauro, and C. D. Lin, Nature (London) **483**, 194 (2012).

[38] J. Xu, C. I. Blaga, A. D. DiChiara, E. Sistrunk, K. Zhang, Z. Chen, A.-T. Le, T. Morishita, C. D. Lin, P. Agostini, and L. F. DiMauro, Phys. Rev. Lett. **109**, 233002 (2012).

[39] A. Čerkić and D. B. Milošević, Phys. Rev. A **75**, 013412 (2007).